Volume 10, Number 1, 2017. pp. 33-48

Jordan Journal of Physics

ARTICLE

Optical and Structural Characterization of Dip Synthesized Al-B Co-doped ZnO Seeded Platforms for ZnO Nanostructures

A. A. Ahmad[a], **A. M. Alsaad**[a], **Q. M. Al-Bataineh**[a], **A. A. Bani-Salameh**[a], **H. M. Al-Khateeb**[a] and **M. A. Al-Naafa**[b]

[a]*Department of Physical Sciences, Jordan University of Science & Technology, P.O. Box 3030, Irbid-22110, Jordan.*
[b]*Department of Chemical Engineering, Ha'il University, Ha'il, Saudi Arabia.*

Received on: 14/11/2016; *Accepted on: 27/2/2017*

Abstract: Zinc oxide and aluminum-boron co-doped zinc oxide (Al-B:ZnO) thin films have been dip coated on glass substrates using Sol-Gel technique. The ZnO solution was prepared by using zinc acetate dihydrate (ZAD) as starting material. Ethanol and citric acid were used as solvent and solution stabilizer, respectively. Doping of Al-B was achieved by adding a proper molar ratio of aluminum nitrate ($Al(NO_3)_3\ 9H_2O$) and boric acid (H_3BO_3) to the final ZnO solution. The optical properties for the films were investigated through the UV-Vis spectrophotometry technique. The transmittance of the undoped ZnO decreases while the concentration of boron increases and increases while the concentration of Al increases over the range of interest. The index of refraction was found to be between 1.73 and 2.43 for the undoped ZnO, which agrees well with that of the bulk ZnO. It increases while the B concentration increases and decreases while the concentration of Al increases. The structural properties were also investigated through XRD, SEM and EDAX measurements. The films acquired hexagonal structure after annealing. The films have been used as seeded platforms for growing ZnO nanostructures using hydrothermal technique and found to fit better for the ZnO platforms rather than the doped ones.

Keywords: Thin films, ZnO, Al-B co-doped ZnO, Sol gel process, Dip coating, Nanostructures, Optical properties, Structural properties.
PACS: 78, 81

Introduction

Zinc oxide (ZnO) thin films are considered the most important metal oxide semiconductors owing to the fact that they have unique features and a wide range of technological applications in various fields, such as solar cells, photovoltaic cells, gas sensors, light emitting devices, photocatalysts and cancer treatment [1]. They have n-type semiconducting property with large excitonic binding energy of around 60 meV and a wide band gap energy of around 3.37 eV at room temperature [2]. They have attracted much interest in the area of photo-electronic devices for high performance of light-emission properties. ZnO thin films have been deposited by various methods, such as magnetron sputtering [3, 4], metal organic chemical vapor deposition [5-7], pulsed laser deposition [8], electrochemical deposition [6] and the sol-gel method [9, 10].

Zinc oxide plays an important role in a wide range of applications, such as microeletromechanical systems (MEMS), due to their good piezoelectric effect [11-13], transparent conducting electrodes in some devices, due to their good electrical conductivity [14], light emitting diodes, UV lasers, transparent field effect transistors and other optical coating applications [15]. ZnO films were usually doped by various doping materials in order to enhance their physical properties, including their optical and electrical characteristics. The physical properties of Al-B

Corresponding Author: A. A. Ahmad **Email**: sema_just@yahoo.com or sema@just.edu.jo

co-doped ZnO thin films have different properties from ZnO thin films [3, 10, 16-18]. Boron and aluminum atoms are known by their low and high atomic numbers (Z_B =5 and Z_{Al} =14), respectively. They have small and large ionic ($_B^{+3}$ and $_{Al}^{+3}$) radii (0.23 Å and 0.535 Å), respectively. Also, they possess large and low electron work functions (4.45 and 4.33 eV), respectively and high and low first ionization energies (8.298 and 5.986 eV) with $2p^1$ and $4s^2$ orbital levels, respectively [7, 19]. Comparing these values to the relevant values for Zn atom (Z_{Zn} = 30, $_{Zn}^{+2}$ radius = 0.23 Å, electron work function of 4.28 eV and first ionization energy of (9.394 eV)), one may recognize that either of the two doping elements (Al or B) will substitute Zn atom in the hexagonal platform [20, 21]. It is well known that the electron affinity for Al (≈ 42 kJ/mol) and that of B (≈ 27 kJ/mol) have larger values than that of Zn atom which has no stable negative ion state. This implies that both Al and B atoms have greater deal of affinity with O atom compared to that of Zn atom during the film growth. Aluminum has greater affinity with oxygen than boron which gives it the priority of substituting zinc with oxygen. Hence, deformed oxides are caused to appear in the films, distorting their physical properties. Post annealing treatment causes microstructural rearrangement, which improves the films' optical properties [22]. Our focus in this research was placed on optimizing the experimental conditions in order to produce ZnO films suitable for specific applications, such as photovoltaic cells, solar cells or optical coatings. The outcomes were obtained by co-doping the ZnO films with Al and B through adjusting their content ratios in order to produce the required characteristics. Our study was devoted to elaborate the effect of Al-B combination on the structural and optical properties of dip coated Al-B co-doped ZnO thin films via sol gel technique on glass substrates and treated with post annealing process. The feasibility of growing ZnO nanostructures on ZnO and Al-B co-doped ZnO seeded platforms was also investigated.

Experimental Procedure

Deposition of ZnO and Al-B Co-doped ZnO Thin Films

The glass substrates were cleaned with soap solution, rinsed with distilled water, dipped in ethanol for 15 minutes and finally dried in air. The undoped ZnO solution was prepared by dissolving 4.38 g of zinc acetate dihydrated ($Zn(CH_3CO_2)_2$ $2H_2O$ with purity of 99.5%) in 50 mL absolute ethanol (99.85%) to get 0.4 M in concentration. The solution (sol) was then mixed thoroughly using a magnetic stirrer for 50 minutes at room temperature until it turned milky (gel). The ethanolamine stabilizer of 1.7 mL was added to the solution in terms of drop by drop while stirring the solution to make it transparent. The resulting mixture was stirred for 40 minutes to get a homogeneous solution. The solution was filtered by paper-filter, 0.45 μm in dimension. The films were dip coated by dipping the substrate in the solution for 2 hours. The films were dried in oven for 15 minutes at 110 ^oC to evaporate the solvents and organic residues. Finally, ZnO films were annealed in air at 500 ^oC for 2 hours [23, 24]. Boric acid (H_3BO_3) and aluminum nitrate ($Al(NO_3)_3$ $9H_2O$) were then added with the desired ratios to the undoped ZnO solution in order to prepare Al-B co-doped ZnO solution. The solution was then mixed by the magnetic stirrer for 30 minutes at room temperature to make it homogeneous. Again, the solution was then filtered by similar paper-filters. The Al-B co-doped ZnO solution was then deposited by dip coating technique for 2 hours on pre-cleaned glass substrates. The deposited Al-B co-doped ZnO films were then treated similar to the undoped ZnO film [24].

Hydrothermal Synthesis of Zno Nanoparticles Technique

All the chemicals used in this work were of analytical reagent grade and used as received from the supplier without any further purification or post-treatment. In a typical procedure, stock solution of zinc acetate dihydrates $Zn(CH_3CO_2)_2$ $2H_2O$ (5 mM) was prepared in 20 mL of ethanol under magnetic stirring. A volume of 20 mL of KOH, prepared by a percentage of 0.2 mM to 0.5 mM in ethanol, was added to the solution under stirring for 30 minutes. The solution was then transferred into a water bath and maintained at a certain temperature in the range of (65 - 82 °C) for 2-3 hours until it formed the roots of nanoparticles. The obtained ZnO nanoparticles (ZnO-NP) were washed three times with ethanol and distilled water in order to remove impurities and then dried in air at 50 °C for 24 hours [25].

Results and Discussion

Optical Properties of the Undoped and the Al-B Co-doped ZnO Thin Films

A dual channel spectrophotometer (Perken Ellmer Lamda-9 series) was used to investigate the optical properties of the undoped and the Al-B co-doped ZnO thin films for various ratios of Al to B concentration in the solution. All the measurements were taken at room temperature. Fig. 1 shows the transmittance for the films deposited under various Al / B concentration ratios. It is clearly seen that the transmittance decreases over the whole range of interest as the concentration of B increases and increases as the concentration of Al increases. This observed fact agrees well with the findings of S. Ilican et al. [26], L. Yang et al. [27] and A. Sreedhar et al. [28]. The transmittance for the undoped ZnO (0.0% / 0.0%) film was found to almost vanish in the UV region (below 375 nm), while it increases much more than that for the Al / B doped ZnO films with 0.25% / 0.25%, 0.25% / 0.50%, 0.50% / 0.25% and 0.50% / 0.50%, respectively. The transmittance increases then abruptly near the band edge to become almost transparent in the visible region. The band gap energy (E_g), defined by the equivalent photon energy related to the average value of transmittance above the band edge and before the film turns transparent in the visible region, was found to be 3.333, 3.374, 3.369, 3.360 and 3.430 eV, respectively. As the Al and B contents were introduced to ZnO solution by small ratios (0.25% for each), no considerable changes have been observed in the transmittance curve in the visible region. However, it increases slightly in the UV region (short dashed curve). E_g was increased to 3.374 eV compared to 3.333 eV for the undoped ZnO film. By introducing 0.50% of both Al and B contents to ZnO solution, the transmittance increases from 85% to around 90% in the visible region and increased much more in the UV region. E_g has increased to 3.430 eV accordingly. By increasing the Al content to 0.50% while fixing B at low ratio (0.25%), E_g increased to 3.360 eV, while the transmittance decreased below 75% in the visible region. However, increasing B ratio to 0.50% while fixing the Al ratio as low as 0.25% increases E_g to 3.3.369 eV and the transmittance increases also to reach around 90% over the visible region. The value of the reflectance was measured by the spectrophotometry technique while using an integrated sphere to reduce the glass effect in the measurements. The argument applied to the transmittance spectra applies to the reflectance spectra as shown in Fig. 2. The reflectance for the undoped ZnO films ranges between 8% and 22% with an average of around 9% in the visible region and peaks at around 385 nm (3.222 eV). The average reflectance increases above that for the undoped ZnO as the B concentration increases to 0.25% or 0.50% while fixing the Al concentration at 25%. However, the average reflectance decreases below that of the undoped ZnO while increasing Al concentration to 25% or 50% at fixed Al concentration of 25%. All the reflectance curves acquire almost similar shape as that for the undoped spectra with varying peak positions and intensity ranges.

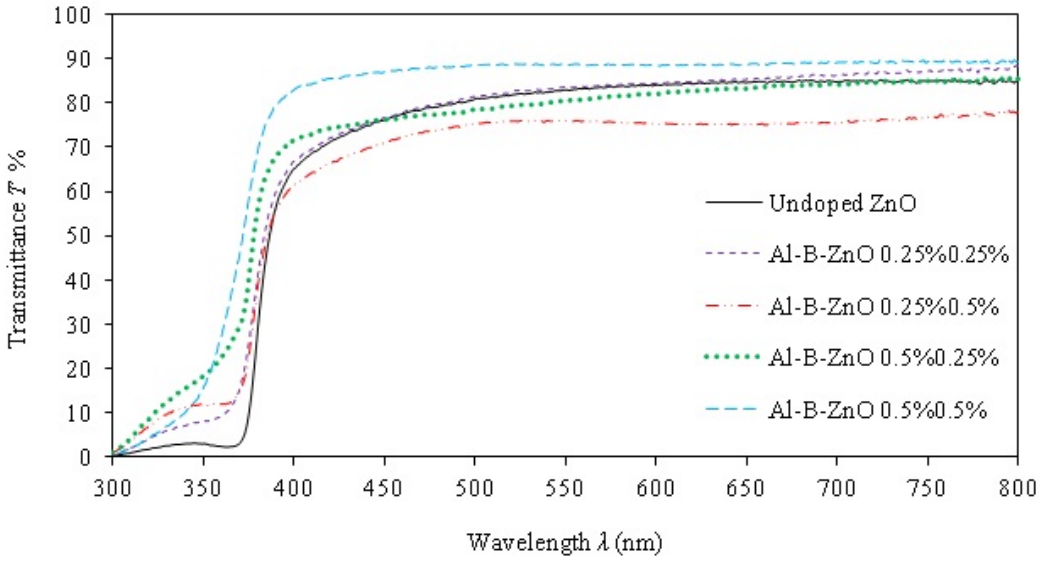

FIG. 1. The transmittance spectra of the undoped ZnO and Al-B co-doped ZnO thin films at various ratios.

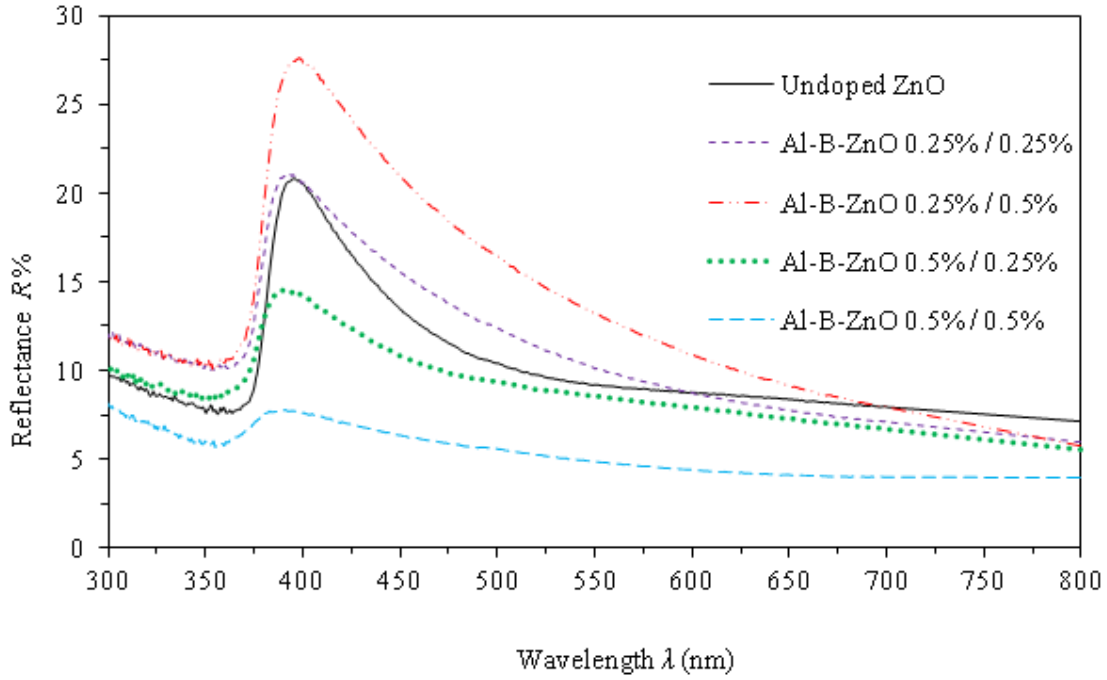

FIG. 2. The reflectance spectra of the undoped ZnO and Al-B co-doped ZnO thin films at various ratios.

In order to investigate the extinction coefficient (k) and the index of refraction (n) of the films, the average thickness was obtained to be about 500 nm by the Scanning Electron Microscopy (SEM) micrograph results. The film thickness was found by calibrated deposition rate which takes 2 hours of deposition to achieve this thickness with non-uniformity of around 2.2%. Fig. 3 shows the extinction coefficient (k) spectra for the films evaluated by $k = \alpha\lambda/4\pi$ over the range of interest, where α is the absorption coefficient [29]. The k values in the visible region increase as the B concentration increases and decrease as Al concentration increases. The curve features of k for the undoped ZnO film show a well-defined peak at around the band gap energy (at λ = 368.5 nm with equivalent E_g = 3.365 eV). When Al and B were introduced to the ZnO solution by 25% for each, the peak value decreased and showed no fine features. It acquires features showing that doping energy levels have been introduced to the band gap near the conduction band (short dashed curve). As the Al and B concentrations have been increased further to 50% for both dopants, the peak feature almost disappeared while the curve steepness has been increased (long dashed curve). Fixing the Al concentration low at 25% while increasing the B concentration up to 50% reduces the value of the peak while still maintaining the overall k curve (dash with two dots) in the normal trend. However, fixing the B concentration low at 25% and increasing the Al concentration up to 50% cause the peak to decrease with lower k values in the UV region (dotted curve). The index of refraction (n) for the thin films has been evaluated from the values of the reflectance and the extinction coefficient as:

$$n = ((1+R)/(1-R)) + \sqrt{((4R/1-R)^2) - k^2}$$

[30-32]. The n value as a function of incident light wavelength is shown in Fig. 4 for all the Al-B co-coped ZnO films compared to that of the undoped ZnO film. The index of refraction for the undoped ZnO (solid line) exhibits values ranging between 1.63 and 2.43 with main peak feature appearing at the beginning of the visible region. As the Al and B concentrations were increased by 25% for both, n increased slightly in the visible region (short dashes). However, as B concentration increases to 50%, n curve increases extremely to reach its maximum value at 2.83 (long dashes with two dots). On the other hand, as Al concentration was increased to 50% while fixing B concentration at 25%, n curve decreased down below that for the undoped ZnO thin film (dotted curve) with an average value of around 1.80. In the case where Al and B contents have been increased to 50% for each, n values reduced between 1.50 and around 1.68 while losing the curve peak feature (long dashes).

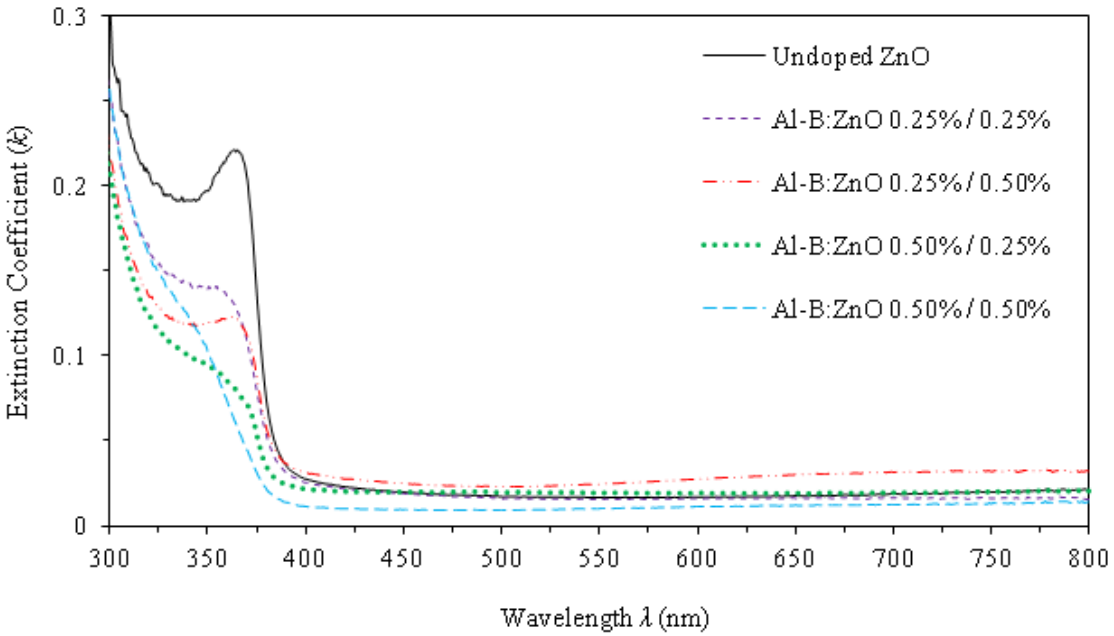

FIG. 3. The extinction coefficient (k) of undoped ZnO and Al-B co-doped ZnO thin films.

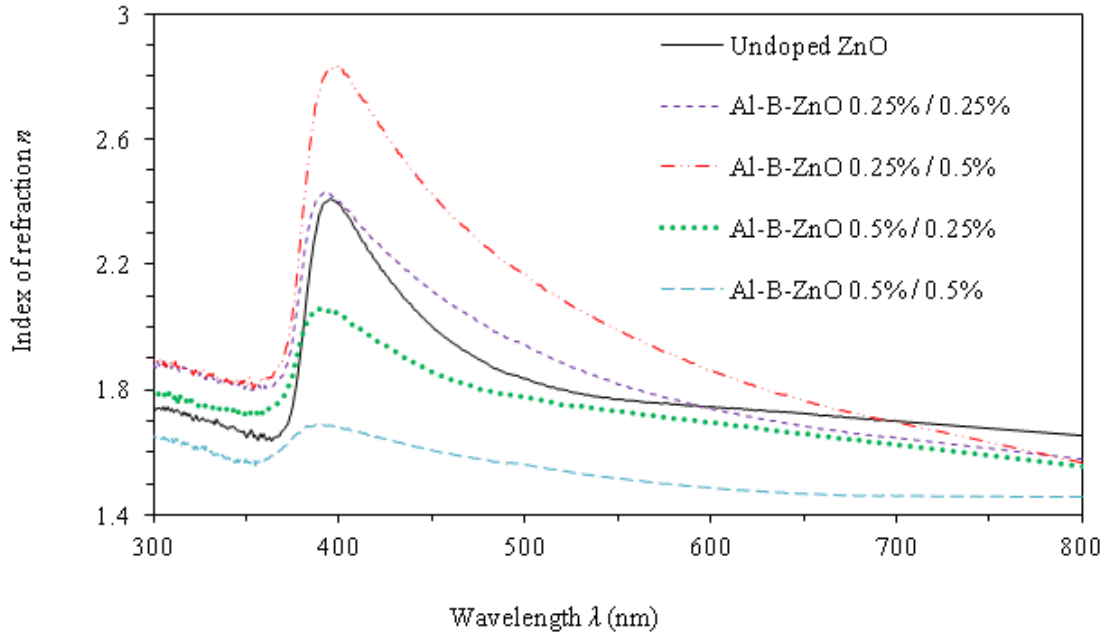

FIG. 4. The index of refraction (n) of undoped ZnO and Al-B co-doped ZnO thin films.

In order to find the film band gap energy (E_g), Tauc plots have been investigated by drawing the relationship between the incident photon energy ($h\upsilon$) and $(\alpha \times h\upsilon)^2$. The absorption coefficient α has been evaluated from the transmittance and the film thickness such that $\alpha = 1/d \ln(1/T)$. Fig. 5 shows Tauc plots for all the deposited films with various Al and B concentrations. E_g was found by extrapolating the linear part of the relationship above the band edge along the incident photon energy axis where $E_g = h\upsilon$. Two main features in Tauc plot were observed while defining the band gap energy for the undoped ZnO film. One transition hub was found at a band gap energy of 3.255 eV, while the other transition feature shows the pronounced band gap energy at 3.362 eV. The

first hub feature indicates the presence of the known excitonic binding energy in ZnO near the band edge. The lower band gap energy (3.255 eV) is related to the donor's level in the pronounced optical band gap (3.362 eV) and the difference between them is related to the electron-hole pair excitonic energy (107 meV). This phenomenon has been observed in many metallic oxide semiconductors such as graphene oxides and tin oxides implanted with carbon ions in addition to ZnO due to the local atomic relaxations around the oxygen vacancies in the neutral, +1 charge and +2 charge states [33-36]. It is well known that the excitonic binding energy for pure crystalline ZnO is around 60 meV at room temperature. However, our films are polycrystalline and non-stoichemetric, which may explain the higher value of excitonic binding energy. Our values are comparable to the values given in the literature for similar deposition process. Table 1 shows all these values for all the deposited films. These features were found for the Al-B co-doped ZnO films with rather lower hub features. Given that the error in E_g is around ± 3.3 x 10-3 eV, the main band gap energy found of the undoped ZnO through using the average transmittance value above the band edge was 3.362 eV as seen in Table 1. As Al and B concentrations become 0.25% for each, E_g decreases to 3.350 eV (3.374 eV from the average transmittance value), while the excitonic energy decreases to 95 meV. Fixing the Al concentration low at 0.25% and increasing the B concentration to 50%, E_g decreases to 3.340 eV (3.369 eV by the transmittance value) and the excitonic energy decreases further to 85 meV. However, fixing the Al concentration high at 0.50% while decreasing the B concentration to 0.25%, E_g increases to 3.368 eV (3.360 eV by the transmittance value) which is around the value for the standard crystalline ZnO material (3.370 eV) [2] and the value of the excitonic binding energy becomes 118 meV. As Al and B concentrations were increased further to 0.50% for each, E_g increased to reach 3.420 eV (3.430 eV by the transmittance value) and the excitonic energy increased to 165 meV. This observation indicates that an increase in Al concentration (at fixed B value) leads to a decrease in the band gap energy, while an increase in B concentration (at fixed Al value) leads to an increase in E_g. This observation is expected, since the grain size increases by increasing the B concentration and decreasing the Al concentration. Our results are consistent with the results in [37, 38]. As mentioned in the introduction, due to the difference in the ionic radii, electron work function and electron affinities of the dopants (Al and B), partial substitutions of either ion (B^{+3} or Al^{+3}) incorporation into the crystalline lattice occur. It is expected that Al^{+3} incorporation occurs more than that of B^{+3} ions. This ultimately leads to domination of the influence of Al-doping on that of B-doping. Further investigation was needed to conclude the efficiency of co-doping ratios including the annealing temperatures and their ambient conditions in order to give an absolute conclusion.

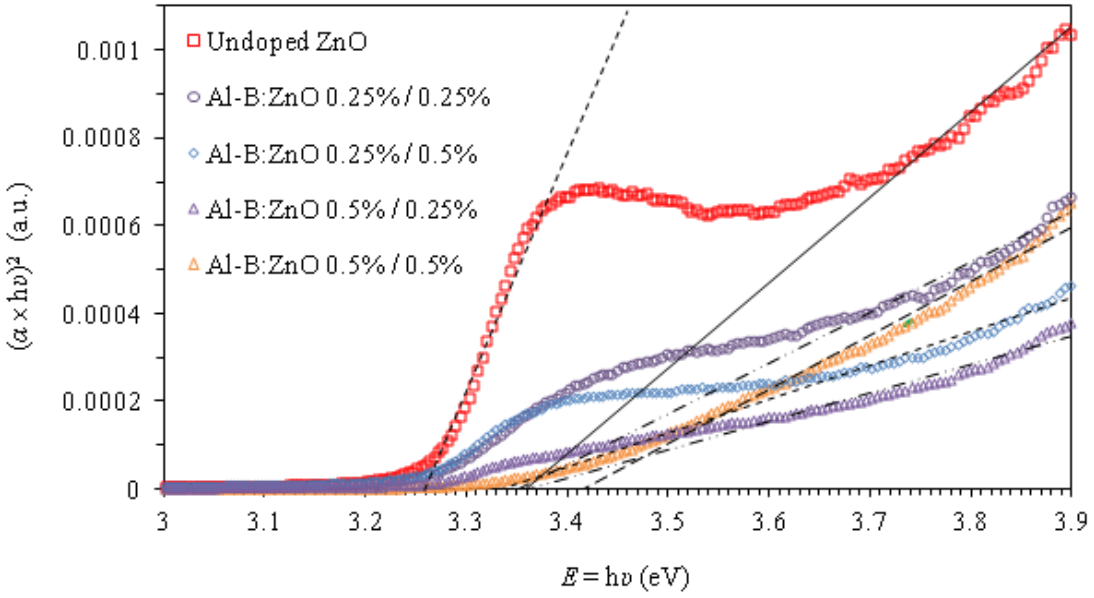

FIG. 5. Tauc optical band gap energy of the dip coated undoped and Al-B-doped ZnO thin films.

TABLE 1. The band gap energy obtained from Tauc plot with its approximated excitonic energy and from the average transmittance value above the band edge for all the samples.

Sample	Tauc E_g (eV)	Excitonic E (meV)	Transmittance E_g (eV)
Undoped ZnO	3.255, 3.362	107	3.333
Al-B:ZnO, 0.25% - 0.25 %	3.350	95	3.374
Al-B:ZnO, 0.25% - 0.50 %	3.340	85	3.369
Al-B:ZnO, 0.50% - 0.25 %	3.368	118	3.360
Al-B:ZnO, 0.50% - 0.50 %	3.420	165	3.430

Wemple-DiDomenico Model

S. H. Wemple and M. DiDomenico [39] have analyzed the refractive index dispersion data below the absorption edge for various covalent and ionic materials in a wide range of different solids and liquids. The analysis was made based on proposing a single effective oscillator model (Wemple and DiDomenico, 1971 [32, 39]), which is a semi-empirical dispersion relation for determining the refractive index n as a function of photon energy as seen in Eq. (1) [23, 30, 36]. The effective single oscillator is characterized by its average excitation energy for electronic transitions (E_o), dispersion energy (E_d) as a measure of the average strength of the optical inter-band transitions, average value of oscillator strength (S_o), oscillator wavelength (λ_o) and the zero frequency or static refractive index (n_o). The index of refraction is defined as [23, 30, 36]:

$$n^2 - 1 = \frac{E_d E_o}{E_o^2 - E^2} \quad . \qquad (1)$$

Plotting $(n^2\text{-}1)^{-1}$ against $(h\nu)^2$ gives the oscillator parameters by fitting the data to a straight line while extrapolating it to the zero frequency as seen in Fig. 6 for all the samples. The equations for the fitted lines are shown in the figure against each Al-B co-doping ratio, showing their intercepts with the vertical axis and their slopes.

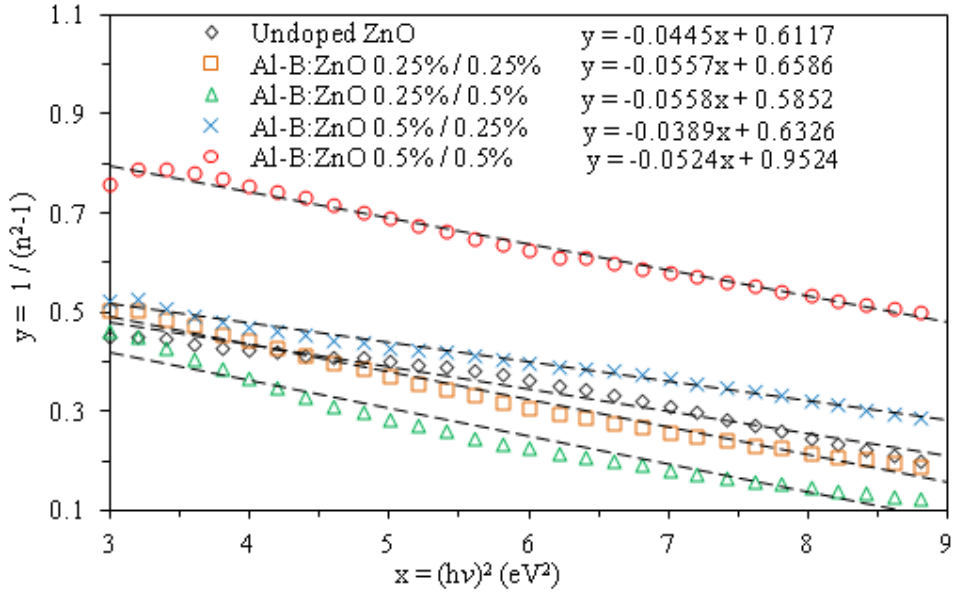

FIG. 6. The relationship between $(n^2\text{-}1)^{-1}$ and $(E = h\nu)^2$ of the single oscillator model for all the Al-B co-doping ratios compared to that for the undoped ZnO film.

The values of E_o and E_d can then be calculated from the slope $(E_oE_d)^{-1}$ and the intercept at the vertical axis (E_o/E_d). The average oscillator wavelength (λ_o) and the oscillator strength (S_o) parameters for all the samples were also determined by the single oscillator model given by Eq. 2 as [23, 30, 36, 39]:

$$n^2 - 1 = \frac{S_o \lambda_o^2}{(1 - \lambda_o^2)/\lambda^2} \quad . \qquad (2)$$

By plotting $(n^2\text{-}1)^{-1}$ against (λ^{-2}), one can obtain the values of the oscillator parameters by fitting the data to a straight line at low frequencies and extrapolating it to the zero frequency as seen in Fig. 7 for all the thin films. The values of S_o and λ_o were obtained from the slopes $(1/S_o)$ and the intercepts $(1/S_o\lambda_o^2)$ at the vertical axis.

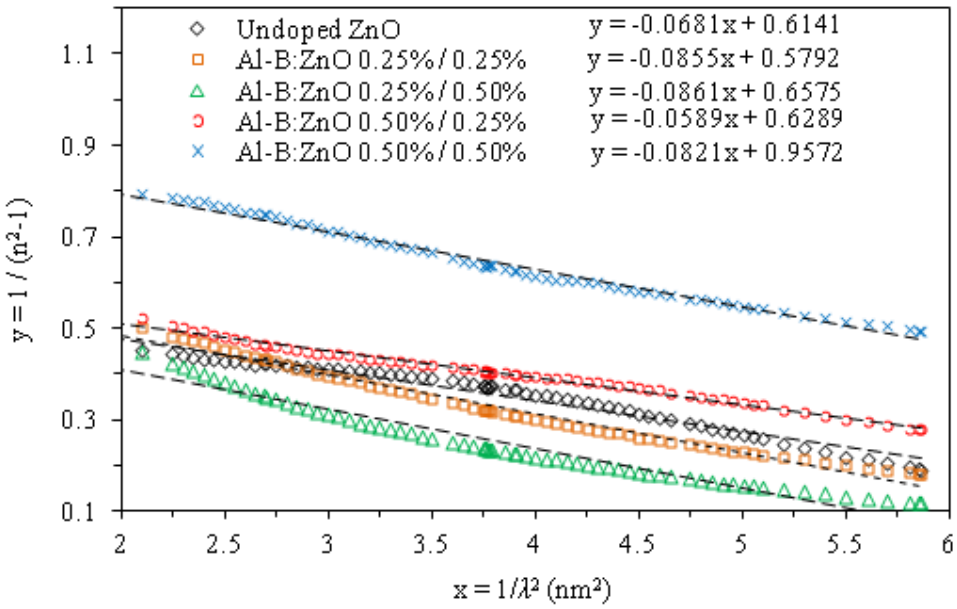

FIG. 7. The relationship between $(n^2\text{-}1)^{-1}$ and (λ^{-2}) of the single oscillator model for all the Al-B co-doping ratios compared to that for the undoped ZnO film.

The static refractive index (n_o) was calculated from Wemple-DiDomenico dispersion parameters (E_o and E_d) using Eq. (3) [23, 30, 36, 39]:

$$n_o = \sqrt{1 + (E_d / E_o)} \ . \qquad (3)$$

The parameters characterizing the average oscillator model proposed by Wemple and DiDomenico [39] representing the light-material interactions are shown in Table 2. It is clearly seen that the average oscillator energy (E_o) was found to be as high as 4.03 or 4.26 eV when Al content was made as high as 0.50% while B content was either 0.25% or 0.50%, respectively. However, E_o value was found to be as low as 3.44 or 3.18 eV when Al content was made as low as 0.25% while B content was made at 0.25% or 0.50%, respectively. E_o for the undoped ZnO film was found to be around the average value (3.73 eV) compared to the values obtained from the extreme values of Al content regardless of boron concentration. This indicates that increasing the Al content in the solution increases E_o, while increasing the B content decreases the value of E_o at low Al concentration (0.25%) and increases it at higher value (0.50%). The dispersion energy (E_d) was also found to be at its minimum value (4.47 eV) when both concentrations for Al and B were maintained high at 0.50% and found to be the highest (6.37 eV) when the B concentration was lowered to (0.250%). However, E_d was found to be at almost the moderate value (5.22 or 5.30 eV) when boron concentration is lowered to 0.25% and Al content was made low (0.25%) or high (0.50%), respectively. E_d for the undoped ZnO film was found to be in between the extreme values (6.10 eV). The static index of refraction (n_o) was found to be at the highest value (1.65) when B concentration was higher (50%) and B concentration at the lowest value (0.25%). n_o was found to be minimum (1.43) when the doping concentration for both Al and B was made at the highest value (0.50%). It was found that n_o increases by decreasing boron at fixed aluminum ratio (0.50%) while it increases (1.59 to 1.65) by increasing B content from 0.25% to 0.50% at the minimum content of Al (0.25%). The oscillator strength S_o was found to be at the highest value (16.98×10^{-5} nm^{-2}) when the Al / B ratios are 0.50% / 0.25% and at the lowest value (11.61×10^{-5} nm^{-2}) when these ratios are reversed (i.e.,0.25% / 0.50%), while its value was found to be around the average of these

extremes (14.68×10^{-5} nm^{-2}) without co-doping. The average wavelength (λ_o) was found to be at the lowest value (8.58 nm) when Al concentration (0.50%) was made higher than B concentration (0.25%). It was found at its highest value (14.76 nm) when the ratios were reversed. Similarly, λ_o was found to be at around the average value (11.09 nm) of these extremes without co-doping. Our results of the undoped ZnO material were found to be consistent with the results seen in the literature for ZnO films as deposited with the DC sputtering at room temperature without annealing, but do not agree with the results found for the films when deposited at higher substrate temperature or treated with post-annealing [23]. Our results of E_o and E_d for the Al-B co-doped thin films were found to be much higher than the results obtained for single doping with Al and comparable with the results obtained for films co-doped with Li-Mg [40, 41]. Our results were found to be comparable to those for ZnO thin films deposited with pure boron [42]. It is clearly seen that the co-doping process by Al and B controls the single oscillator's parameters above and below each corresponding parameter for the undoped ZnO film. From the material processing point of view, this indicates that the optical, and hence the electrical as well as the micro-structural characteristics can be controlled. This achievement is due to the fact that controlling the co-doping ratios for Al and B controls the physical properties of the films. It shows that co-doping (by Al and B) gives the benefit over singular doping (by either Al or B) through better control of the film characteristics.

TABLE 2. The parameters obtained for the average single oscillator model proposed for Wemple-DiDomenico model representing the light-material interactions.

Sample	E_o (eV)	E_d (eV)	n_o	$S_o \times 10^{-5}$ (nm^{-2})	λ_o (nm)
Undoped ZnO	3.73	6.10	1.62	14.68	11.09
Al-B:ZnO, 0.25% / 0.25 %	3.44	5.22	1.59	11.70	14.76
Al-B:ZnO, 0.25% / 0.5 %	3.18	5.30	1.65	11.61	13.10
Al-B:ZnO, 0.50% / 0.25 %	4.03	6.37	1.61	16.98	9.36
Al-B:ZnO, 0.50% / 0.50 %	4.26	4.47	1.43	12.18	8.58

Structural Properties for the Un-doped and the Al-B Co-doped ZnO Thin Films

It was found that annealing the films under atmospheric pressure at 500 ^oC for two hours produces the best crystalline features [24]. All samples were treated similarly. Fig. 8 shows the X-ray diffraction patterns for the undoped and the Al-B co-doped ZnO thin films. It shows the X-ray diffraction patterns with the peaks observed at Bragg's angles for the undoped ZnO film at 31.496^o, 34.173^o and 35.994^o which belong to the hexagonal crystalline orientations for Miller indices of (100), (002) and (101) planes, respectively. The lattice parameters for ZnO thin films evaluated by XRD patterns (see Table 3) are in good agreement with standard values for the ZnO thin films reported by the Joint Committee on Powder Diffraction Standards (JCPDS 36-1451) [43]. The crystallinity was improved in favor of the (002) orientation when B concentration was made dominant (50%) in the ZnO solution, while the Al concentration was made low at 25%. It was found that the most crystalline features occur preferring the (002) orientation when Al concentration was dominant (50%) while B concentration was low (25%). It is worth mentioning that small peaks have appeared, mainly in the non-doped ZnO film, in relevance to the planes defined by the Miller indices (102), (110), (103) and (112), respectively. These peaks indicate that the materials deposited under our experimental conditions were polycrystalline in nature. They gradually weakened by varying the co-doping ratios until they disappeared at higher concentrations of Al and B (0.50% for each).

TABLE 3. The lattice parameters of ZnO thin film annealed at 500 °C for 2 hours.

a (Å)		c (Å)	
Calculated	Standard	Calculated	Standard
3.279	3.250	5.246	5.207

Table 4 shows the lattice constants and the structural parameters for all samples. Low concentrations (25%) for both dopants (Al and B) did not change the grain size, the dislocation and the strain compared to those for undoped ZnO film. The grain size was found to increase (21.872 nm), while the dislocation and strain were found to decrease to 20.903 × 10^{14} (lines/m^2) and 1.611 ×10^{-3}, respectively when B concentration was dominant (50%) while Al concentration was low (25%). However, the grain size was found to decrease (17.895 nm), while the dislocation and strain were found to increase to 31.226 × 10^{14} (lines/m^2) and 1.969 ×10^{-3} when Al concentration was dominant (50%) and B concentration was low (25%). The rough decrease in the grain size (16.404 nm), the huge increase in the dislocation (37.161× 10^{14} (lines/m^2)) and the rough increase in strain (2.148 ×10^{-3}), respectively occur when both dopants (Al and B) were increased in ratios to 50% for each. One can recognize the changes in strain causes relevant changes in the lattice parameters, accordingly.

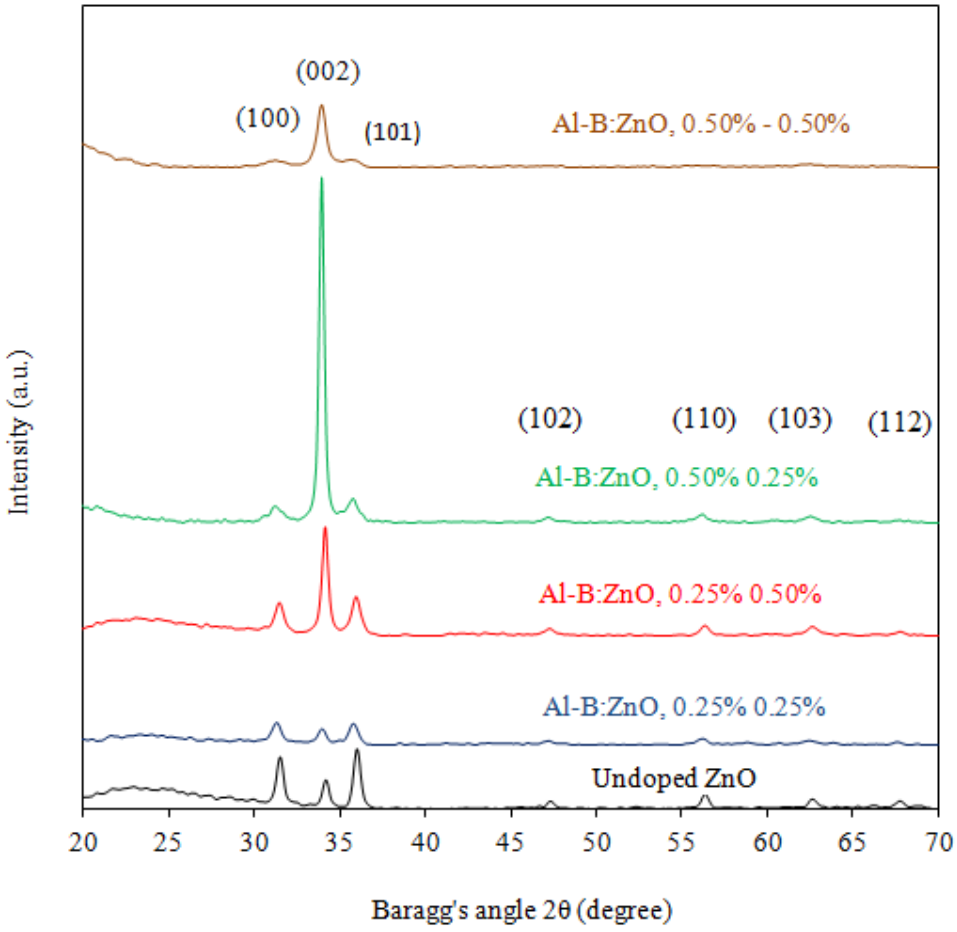

FIG. 8: The X-ray diffraction patterns of thin films with various concentrations of Al and B.

TABLE 4. The lattice parameters and structural parameters for thin films annealed at 500 °C for 2 hours.

Sample	Lattice Parameters		Grain size	The dislocation density δ	Strain ε
	a (Å)	c (Å)	D (nm)	(× 10^{14}) (lines/m^2)	(×10^{-3})
Undoped ZnO	3.279	5.246	19.684	25.806	1.790
Al-B:ZnO, 0.25 - 0.25	3.299	5.279	19.684	25.806	1.790
Al-B:ZnO, 0.25 - 0.50	3.283	5.252	21.872	20.903	1.611
Al-B:ZnO, 0.50 - 0.25	3.246	5.283	17.895	31.226	1.969
Al-B:ZnO, 0.50 - 0.50	3.307	5.283	16.404	37.161	2.148

SEM Micrographs

The Scanning Electron Microscope micrographs have been used to investigate the surface morphologies of the films for the undoped ZnO and the Al-B co-doped ZnO films. Fig. 9 shows the SEM micrographs for the undoped ZnO and the Al-B co-doped ZnO (0.25% / 0.25%, 0.25% / 0.50%, 0.50% / 0.25% and 0.50% / 0.50% of Al-B contents, respectively) thin films. Undoped ZnO film exhibits a smooth surface with very small crystalline grains as seen in the large-scale micrograph (20 µm scale) of Fig. 9(a). The grain features were found to be so fine and they look very uniform as seen on the short-range scale (5µm scale) of Fig. 9(b). As Al and B were introduced to the film, the micrograph of the film surface varied accordingly. Fig. 9 (c) shows the micrograph for the film surface for low concentrations of both Al and B (25%). It is clearly seen that big clusters of ZnO oxides (white colors) are observed on the surface with no much regularity. As B concentration becomes dominant (50%), the clusters were observed to disseminate, forming a solid surface of Al-B co-doped beneath rough grains (black color) as seen in Fig. 9(d). As Al becomes dominant (50%), Al-B co-doped ZnO grains become finer and clear (as seen in Fig. 9(e)) with even shorter scale (500 nm). This agrees well with the X-ray diffraction patterns, where the grain size increases as B content increases, while it decreases as Al content increases. Finally, when both of Al and B contents increase to 50% for each, the film surface looks fine and almost completely compensated from the residuals of zinc and oxides by the additives of Al and B as seen in Fig. 9(f).

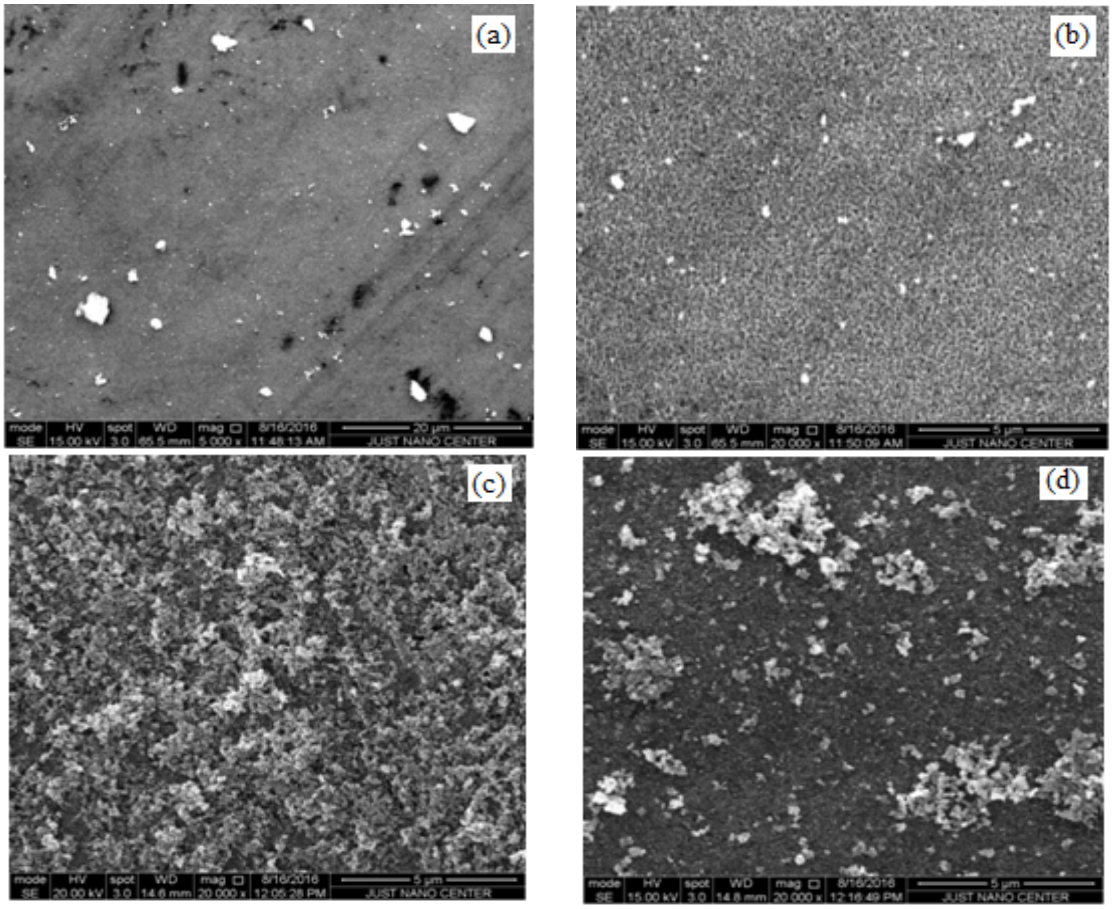

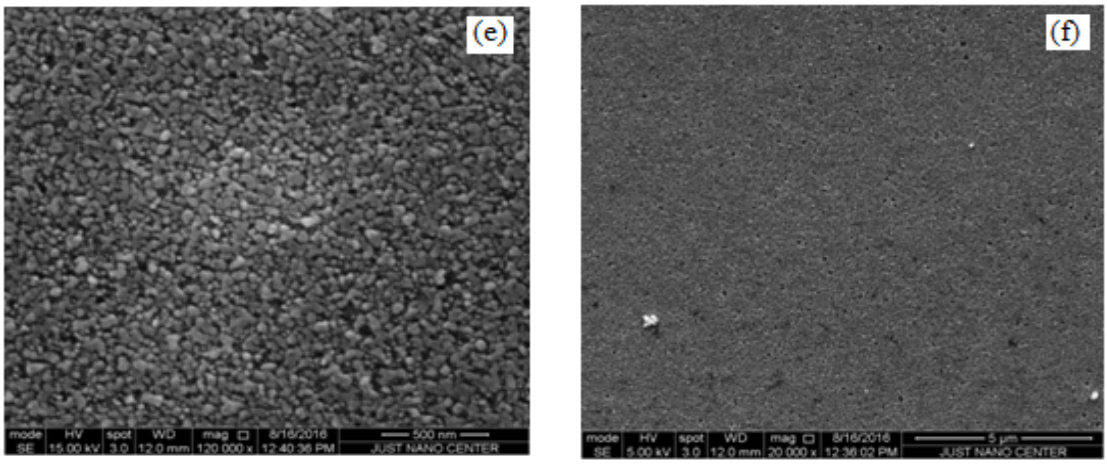

FIG. 9. The SEM micrographs of the undoped ZnO with (a) large scale (20 μm) and (b) short scale (5 μm) in addition to Al-B co-doped ZnO thin film with (c) 0.25% - 0.25%, (d) 0.25% - 0.50%, (e) 0.50% - 0.25% and (f) 0.50% - 0.50% concentrations, respectively.

Deposition of ZnO Nanoparticles on Seeding Platforms by Hydrothermal Deposition

ZnO nanoparticles (NP) were grown on undoped or Al-B co-doped ZnO thin films used as host seeded-platforms. The platforms were deposited on glass substrates as discussed in the previous sections. The ZnO-NPs were grown by hydrothermal process. Figs. 10(a) and (b) show the surface of small sizes (around 50 nm) of aggregated ZnO-NPs grown on undoped ZnO thin film in large-scale (1 μm) and in short-scale (500 nm) micrographs, respectively. The films were found to be suitable for growing the ZnO-NPs with uniform morphology. Attempts of growing ZnO-NPs on Al-B co-doped ZnO seeded platforms with 0.25% for each doping element produce cloudy diffused clustered-forms of NPs ranging from 100 nm to 250 nm as seen in Fig. 10(c). When B content becomes the dominant doping element (0.50%), the cloudy nanostructures diffuse into fine and soft dissociated NPs as seen in Fig. 10(d). However, as Al becomes the dominant doping element (0.50%), small sizes of hexagonal shape NPs (around 100 nm) were observed to aggregate on the surface as seen in Fig. 10(e). It is worth mentioning that this combination of co-doing produces the best films of hexagonal crystalline microstructure with (002) preferred orientation as seen in the X-ray diffraction (XRD) patters (Fig. 8). It is clearly seen that this form of Al-B co-doped ZnO seeded platforms showed the best combination in hosting good growth of NPs. As the platform becomes rich with both Al and B (50% for each), the grown nanostructure becomes nonuniformly cloudy with no distinct homogeneous structure as seen in Fig. 10 (f).

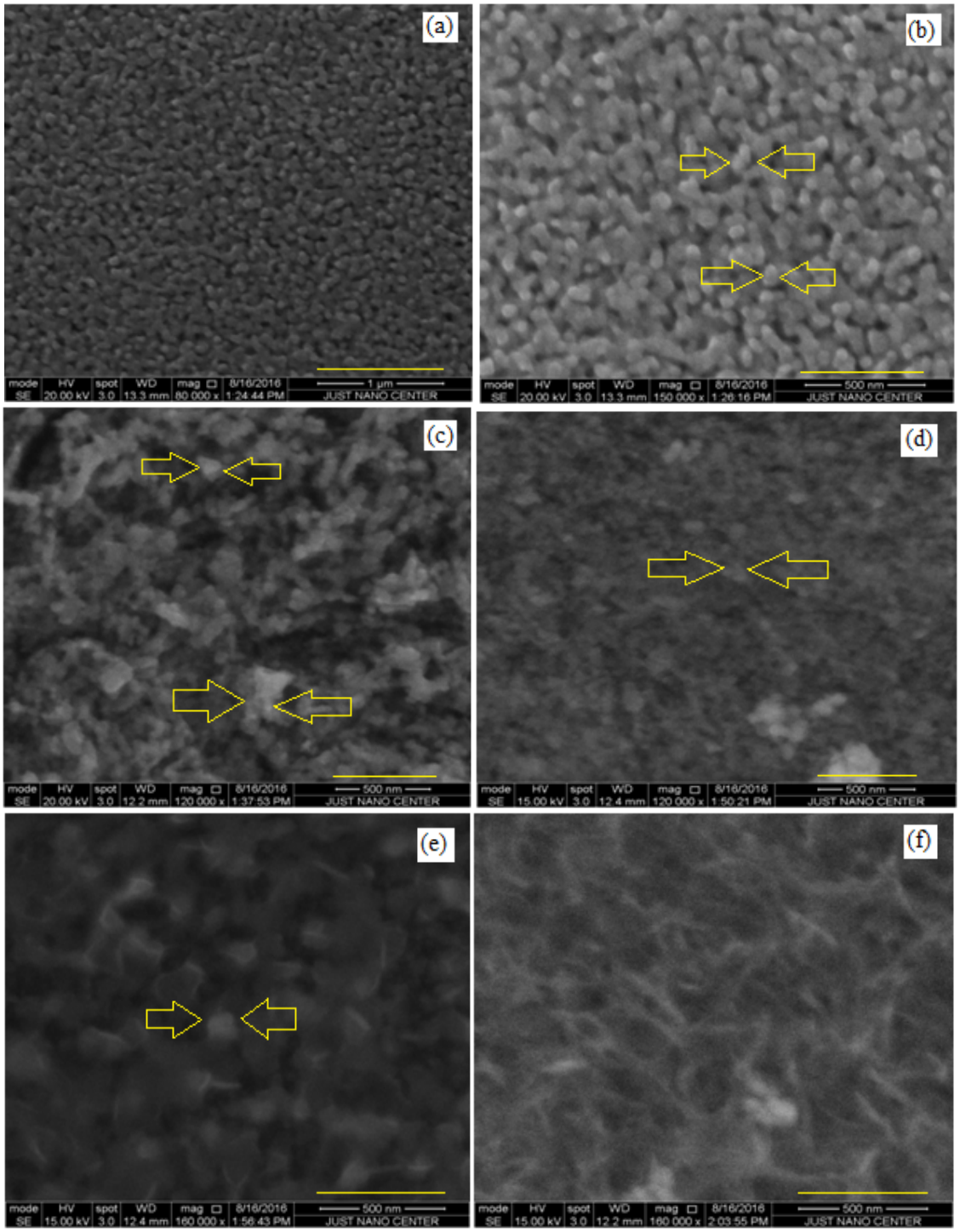

FIG. 10. The SEM micrographs of ZnO-NPs on seeded undoped ZnO platforms in (a) large scale (1μm) and (b) short scale (500 nm) and Al-B co-doped platforms with (c) 0.25% - 0.25%, (d) 0.25% - 0.5%, (e) 0.50% - 0.25% and (f) 0.50% - 0.50% concentrations, respectively.

Conclusions

Undoped ZnO thin films have been prepared by sol gel using dip coating technique. The zinc acetate dihydrate (Zn $(CH_3CO_2)_2$ $2H_2O$) with 99.5% of purity was used as a starting material dissolved with ethanol, while mono-ethanolamine was used as a stabilizer. Al-B co-doped ZnO thin films have been prepared by using the ZnO solution in addition to boric acid (H_3BO_3) and aluminum nitrate ($Al(NO_3)_3$ $9H_2O$) to form the final ZnO solvent. The various molar ratios of boric acid / aluminum nitrate used in the solutions were 0.0% / 0.0%, 0.25% / 0.25%, 0.25% / 0.50%, 0.50% / 0.25% and 0.50% / 0.5%, respectively.

The transmittance and reflectance were investigated and the index of refraction, extinction coefficient and optical band gap energy have been evaluated accordingly. The average transmittance of the undoped ZnO thin film was found to be around (>80%) in the visible region. The transmittance reduces, in a curve-trend measure, by increasing the B concentration and increases by decreasing the Al concentration. The relevant optical properties were also affected accordingly. The index of refraction was found to range between 1.63 and 2.43 for the undoped ZnO films. The optical band gap energy for the undoped deposited ZnO thin film was found to be about 3.362 eV (3.333 eV from the transmittance). These values agree well with that for the bulk ZnO (3.40 eV) and for the thin films (3.37 eV). The E_g value was found to decrease while increasing the concentration of Al and decrease while increasing the B content in the solution. This fact supports the prediction that the optical band gap energy decreases while the grain size increases in the films. As the film becomes rich with both Al and B, E_g increases to 3.430 eV, indicating that complete compensation for zinc and oxygen vacancies has been almost achieved by the presence of Al and B. The higher partial ionic substitution of Al^{+3} incorporation in the lattice structure, compared to that of B^{+3} ion, leads to domination of its influence on the optical and structural properties of the co-doped thin films with still minor influence of B on the microstructure. However, further investigation is needed to conclude the efficiency of co-doping ratios including the annealing temperatures and their ambient conditions.

The films' microstructure has been investigated using XRD. The analysis revealed a polycrystalline microstructure before being treated with post-annealing, while the microstructure has been enhanced to almost single orientation by proper annealing temperature (500 ^oC) for a proper period of time (2 hours). Undoped ZnO thin film demonstrated a hexagonal wurtzite structure. The lattice constants were calculated and found to agree well with that for the bulk ZnO material. The crystalline grain size for the undoped ZnO film was found to be around 20 nm. The grain size increases by increasing the concentration of B and decreases by increasing the content of Al in the films. This fact confirms the predicted result of increasing the grain size being associated with decreasing the optical band gap energy. The SEM micrographs indicate that the morphology of the film surface depends on the B and Al concentrations. It was found that using the undoped ZnO thin film as the host seeded platform to grow fine and uniform ZnO-NPs is feasible with an average particle size of around 20 nm. However, introducing boron to the ZnO platform disturbs the regularity of the NPs aggregation. Low ratio of boron concentration leads to the formation of huge clusters, while increasing the boron ratio diffuses the clusters' density while bowing the size to form irregular nanoclouds at higher boron concentration. Aluminum-rich seeded platforms produce hexagonal NPs with an average size of 100 nm.

Acknowledgments

The authors would like to thank Jordan University of Science and Technology for the support provided by the Deanship of Scientific Research. The authors would also like to thank Prof. Borhan Albiss and Prof. M-Ali Al-Akhras for their help in using the facilities of the Center of Nanotechnology and the Lab. of Biomedical Physics.

References

[1] Shampa, M., "Preparation of Undoped and Some Doped ZnO Thin Films by Silar and Their Characterization", (Department of Physics, University of Bardhaman, Bardhaman, India, 2014).

[2] Karpina, V., Lazorenko, V., Lashkarev, C., Dobrowolski, V., Kopylova, L., Baturin, V., Pustovoytov, S., Karpenko, A.J., Eremin, S. and Lytvyn, P., Crystal Research and Technology, 39 (2004) 980.

[3] Wong, L.H. and Lai, Y.S., Thin Solid Films, 583 (2015) 205.

[4] Wen, B., Liu, C., Wang, N., Wang, H., Liu, S., Jiang, W., Ding, W., Fei, W. and Chai, W., Applied Physics A, 121 (2015) 1147.

[5] Liu, Y., Li, Y. and Zeng, H., Journal of Nanomaterials, 2013 (2013).

[6] Tsin, F., Venerosy, A.L., Vidal, J., Collin, S.P., Clatot, J., Lombez, L., Paire, M., Borensztajn, S., Broussillou, C.D., Grand, P.P., Jaime, S., Lincotm D. and Rousset, J., "Electrodeposition of Zno Window Layer for an All-Atmospheric Fabrication Process of Chalcogenide Solar Cell", Scientific Reports, The Author(s), (2015) p. 8961.

[7] Lee, J.H. and Park, B.O., Thin Solid Films, 426 (2003) 94.

[8] Kaur, G., Mitra, A. and Yadav, K., Progress in Natural Science: Materials International, 25 (2015) 12.

[9] Kim, S., Yoon, H., Kim, D.Y., Kim, S.O. and Leem, J.Y., Optical Materials, 35 (2013) 2418.

[10] Wen, B., Liu, C.Q., Wang, N., Wang, H.L., Liu, S.M., Jiang, W.W., Ding, W.Y., Fei, W.D. and Chai, W.P., Chinese Journal of Chemical Physics, 29 (2016) 229.

[11] Minne, S., Manalis, S. and Quate, C., Applied Physics Letters, 67 (1995) 3918.

[12] Liu, C., Yu, A., Peng, M., Song, M., Liu, W., Zhang, Y. and Zhai, J., The Journal of Physical Chemistry C, 120 (2016) 6971.

[13] Li, Y., Gao, Z., Qin, W., Wen, Q. and Jun, M., Biochem. Anal. Biochem., 5 (2016) 2161.

[14] Eberspacher, C., Fahrenbruch, A.L. and Bube, R.H., Thin Solid Films, 136 (1986) 1.

[15] Natsume, Y. and Sakata, H., Thin Solid Films, 372 (2000) 30.

[16] Kumar, V., Singh, R., Purohit, L. and Mehra, R., Journal of Materials' Science & Technology, 27 (2011) 481.

[17] Ammaih, Y., Lfakir, A., Hartiti, B., Ridah, A., Thevenin, P. and Siadat, M., Optical and Quantum Electronics, 46 (2014) 229.

[18] Jagadamma, L.K., Al-Senani, M., El-Labban, A., Gereige, I., Ndjawa, N., Guy, O., Faria, J.C., Kim, T., Zhao, K. and Cruciani, F., Advanced Energy Materials, 5 (2015).

[19] Chen, J., Chen, D. and Chen, Z., Science in China, Series E: Technological Sciences, 52 (2009) 88.

[20] K.B.P.T.o.E.-S.b.I.R. Environmental Chemistry.com, http://EnvironmentalChemistry.com/yogi/periodic/ionicradius.html (1995 - 2017).

[21] Boundless, Boundless Chemistry, https://www.boundless.com/chemistry/textbooks/boundless-chemistry-textbook/atoms-molecules-and-ions-2/the-periodic-table-35/the-periodic-table-203-3515/.

[22] Gupta, C.A., Mangal, S. and Singh, U.P., Applied Surface Science, 288 (2014) 411.

[23] Al-Sanableh, A., "Structural and Optical Properties of ZnO Thin Films Deposited by Sol Gel Coating Technique", (Physics Department, Jordan Univesity of Science and Technology, Irbid, 2006).

[24] Bataineh, Q.M., "Optical and Structural Characterization of Sol-Gel B-ZnO and ZnO Thin Films Used As Seeded Platform for Nanostructured ZnO", (Physics Department, Jordaon Univesity of Science and Technology, 2016).

[25] Sreedhar, A., Kwon, J.H., Yi, J. and Gwag, J.S., Ceramics International, 42 (2016) 14456.

[26] Ilican, S., Yakuphanoglu, F., Caglar, M. and Caglar ,Y., Journal of Alloys and Compounds, 509 (2011) 5290.

[27] Yang, L., Zhang, Y.P., Xu, J.W. and Wang, H., Applied Mechanics and Materials, Trans. Tech. Publ., (2014) 1280.

[28] Sreedhar, A., Kwon, J.H., Yi, J. and Gwag, J.S., Ceramics International (2016).

[29] Ahmad, A.A. and Omari, A.M., International Conference on Advanced Materials (ICAM 2015) IOP Publishing, IOP Conf. Series: Materials Science and Engineering, 92, 012024, IOP Publishing, Irbid, Jordan, 2015, p. 012024.

[30] Ahmad, A.A., Alsaad, A.M., Albiss, B.A., Al-Akhras, M.A., El-Nasser, H.M. and Qattan, I.A., Physica B: Condensed Matter, 470 (2016) 21.

[31] Ahmad, A. and Alsaad, A., The European Physical Journal B-Condensed Matter and Complex Systems, 52 (2006) 41.

[32] Ahmad, A.A., Albiss, B.A., Al-Akhras, M.A., El-Nasser, H.M. and Qattan, I.A., Thin Solid Films, 606 (2016) 133.

[33] Hsu, H.C., Shown, I., Wei, H.Y., Chang, Y.C., Du, H.Y., Lin, Y.G., Tseng, C.A., Wang, C.H., Chen, L.C. and Lin, Y.C., Nanoscale, 5 (2013) 262.

[34] Janotti, A. and Van de Walle, C.G., Reports on Progress in Physics, 72 (2009) 126501.

[35] Impellizzeri, G., Scuderi, V., Romano, L., Napolitani, E., Sanz, R., Carles, R. and Privitera, V., Journal of Applied Physics, 117 (2015) 105308.

[36] Ahmad, A.A., Ianno, N.J., Snyder, P.G., Welipitiya, D., Byun, D. and Dowben, P.A., Journal of Applied Physics, 79 (1996) 8643.

[37] Guillen, C. and Herrero, J., Vacuum, 84 (2010) 924.

[38] Elizabeth, U., Uno, E.O., Sobechukwu, M.C., Olusunle, S.O.O. and Okwuego, E.C., American Journal of Energy Science, 3(4) (2016) 21.

[39] Wemple, S. and DiDomenico Jr, M., Physical Review B, 3 (1971) 1338.

[40] Kim, M.S., Yim, K.G., Son, J.S. and Leem, J.Y., Bulletin of the Korean Chemical Society, 33 (2012) 1235.

[41] Aksoy, S., Caglar, Y., Ilican, S. and Caglar, M., Journal of Alloys and Compounds, 512 (2012) 171.

[42] Hasan, N.A., Abbas, A.A. and Mohammed, J.S., Diyala Journal for Pure Sciences, 12 (2016) 70.

[43] Sarma, H. and Sarma, K.C., Int. J. Sci. Res. Publ., 4 (2014) 1.